

Wavelet-based feature extraction for automatic defect classification in strands by ultrasonic structural monitoring

Piervincenzo Rizzo[†] and Francesco Lanza di Scalea[‡]

*NDE & Structural Health Monitoring Laboratory, Department of Structural Engineering,
University of California, San Diego, 9500 Gilman Drive, M.C. 0085, La Jolla, CA 92093-0085, USA*

(Received May 3, 2005, Accepted October 14, 2005)

Abstract. The structural monitoring of multi-wire strands is of importance to prestressed concrete structures and cable-stayed or suspension bridges. This paper addresses the monitoring of strands by ultrasonic guided waves with emphasis on the signal processing and automatic defect classification. The detection of notch-like defects in the strands is based on the reflections of guided waves that are excited and detected by magnetostrictive ultrasonic transducers. The Discrete Wavelet Transform was used to extract damage-sensitive features from the detected signals and to construct a multi-dimensional Damage Index vector. The Damage Index vector was then fed to an Artificial Neural Network to provide the automatic classification of (a) the size of the notch and (b) the location of the notch from the receiving sensor. Following an optimization study of the network, it was determined that five damage-sensitive features provided the best defect classification performance with an overall success rate of 90.8%. It was thus demonstrated that the wavelet-based multi-dimensional analysis can provide excellent classification performance for notch-type defects in strands.

Keywords: multi-wire strands; guided ultrasonic waves; damage index; feature extraction; discrete wavelet transform; artificial neural networks.

1. Introduction

High-strength, multi-wire strands are widely used in civil engineering such as in prestressed concrete structures and in cable-stayed and suspension bridges. Material degradation of the strands, usually consisting of indentations, corrosion or even fractured wires, may result in a reduced load-carrying capacity of the structure that can lead to collapse. In a survey involving the study of more than one hundred stay-cable bridges Watson and Stafford (1988) pessimistically reported that most of them were in danger mainly because of cable defects. Strand failures that caused bridge collapses were documented in Wales (Woodward 1988), Palau (Parker 1996a, b), and North Carolina (Chase 2001). Hence the need for developing monitoring systems for strands that can detect, and possibly quantify, structural defects.

One monitoring technique under investigation by several researchers uses Guided Ultrasonic Waves (GUWs) that exploit the natural waveguide geometry of the strands. Structural monitoring methods based on GUWs have the potential for both defect detection and stress monitoring. GUWs were used

[†]Assistant Project Scientist, Corresponding Author, E-mail: prizzo@soe.ucsd.edu

[‡]Associate Professor, E-mail: flanza@ucsd.edu

for the detection of defects in multi-wire strands (Kwun and Teller 1994, 1995, Pavlakovic, *et al.* 1999, 2001, Beard, *et al.* 2003) and for the evaluation of stress levels in post-tensioning rods and multi-wire strands (Kwun, *et al.* 1998, Chen and Wissawapaisal 2001, 2002, Washer, *et al.* 2002). The authors have used GUWs for defect detection and stress monitoring in seven-wire steel and composite strands (Rizzo and Lanza di Scalea 2001, 2004a, 2004b, 2005a, Lanza di Scalea, *et al.* 2003). GUV monitoring of embedded, rather than free bars and strands has been a special focus of the NDE group at the Imperial College in London (Pavlakovic, *et al.* 1999, 2001, Beard, *et al.* 2003). GUV monitoring of the interface between steel rebars and surrounding concrete has been examined by the University of Arizona (Na and Kundu 2002, Na, *et al.* 2003).

In addition to the theoretical models and the experimental validations of GUV propagation in strands, improvements are also needed in signal processing, particularly for the extraction of the defect-related features to be used as damage indicators. The goal of the feature extraction is to enhance the monitoring performance in terms of defect detection, sizing and location. Statistical features of vibrational or ultrasonic signals, among which the root mean square, the variance and the kurtosis, have been used successfully for damage detection by Sohn, *et al.* (2001) and Staszewski, *et al.* (2004). Traditionally these features are extracted in the time domain or in the frequency domain.

Features extracted in the joint time-frequency domain are also being considered. One effective joint time-frequency analysis is the Discrete Wavelet Transform (DWT), that is particularly suitable for fast data processing. Compared to the Continuous Wavelet Transform that is not computationally efficient, the DWT can be performed in real-time owing to the existence of a fast orthogonal wavelet transform based on a set of filter banks (Mallat 1999). A recent review of wavelet transforms for damage detection in structures was given by Kim and Melhem (2004). The two outcomes of DWT processing are data denoising and data compression, which have made such processing attractive in various structural health monitoring applications (Abbate, *et al.* 1997, Staszewski 1998, 2002, McNamara and Lanza di Scalea 2004, Rizzo and Lanza di Scalea 2005a). For GUV monitoring, the preferred application of DWT analysis has been the decomposition of Lamb waves for detecting impact damage in fiber-reinforced composite plates (Staszewski, *et al.* 1997, 2004, Paget, *et al.* 2003).

The damage-sensitive features can be naturally coupled to an automatic classification algorithm able to determine the size and the location of the defects. This type of quantitative information may result from a classification based on supervised learning, such as that performed by the popular Artificial Neural Networks (ANNs) that are able to learn from training samples through iterations.

The present paper builds on the basic technique for detecting damage in strands that uses magnetostrictive ultrasonic transducers to excite and detect GUWs. Different features are extracted from GUV signals that are reflected from a notch defect, cut at different depths. The features extracted after the DWT processing prove more sensitive to damage size and more robust against noise than the more conventional features extracted from the time domain or the frequency domain. A multi-dimensional damage index vector is then built and used as the input to an artificial neural network based on the backpropagation algorithm. The network provides automatic classification of the notch size and the notch location. It is shown that appropriate combinations of the signal features and other network parameters can produce excellent defect classification performances.

2. The discrete wavelet transform

For the sake of completeness a brief overview of the DWT is given. A more detailed discussion of the

DWT analysis applied to GUV signals of the type considered in this study was given by Rizzo and Lanza di Scalea (2005a). The DWT may be intuitively considered as a decomposition of a function following hierarchical steps (levels) of different resolutions. At the first step the function is decomposed into wavelet coefficients; low-frequency components (low-pass filtering) and high-frequency components (high-pass filtering) of the function are retained. The signal is therefore decomposed into separate frequency bands (scales). The filtering outputs are then downsampled. The number of wavelet coefficients for each branch is thus reduced by a factor of 2 such that the total number of points at a given level is that of the original signal. Each level j corresponds to a dyadic scale 2^j at the resolution 2^{-j} . It should be mentioned that a perfect dyadic decomposition is only achieved when the Haar mother wavelet is employed. This is due to the so-called “boundary problem.” Furthering the decomposition means increasing the scale that corresponds to zooming into the low-frequency portions of the spectrum.

De-noising and compression of the original signal can be achieved if only a few wavelet coefficients representative of the signal are retained and the remaining coefficients, related to noise, are discarded. In the reconstruction process, the coefficients are upsampled to regain their original number of points and then passed through a reconstruction lowpass filter and reconstruction highpass filter. The reconstruction filters are closely related but not equal to those of the decomposition tree. In the pruning process, the reconstruction by using the decomposition level k (scale 2^k), for example, is achieved by setting the wavelet coefficients from other levels equal to zero.

It is important to emphasize that the success of a proper DWT decomposition is dependent on choosing a mother wavelet that best matches the shape of the signal that is being analyzed.

A thresholding step can be used after the pruning process to further increase the signal-to-noise ratio SNR (Abbate, *et al.* 1994, 1997). In this case, the threshold is applied to the magnitude of the coefficients that are retained. This step assumes that the smaller coefficients represent noise, and can be safely omitted.

The thresholding process enhances the compressing ability of the DWT (Abbate, *et al.* 1994, 1997, Rizzo and Lanza di Scalea 2004b). Signal compression eases data storage and transmission. Ultrasonic signals can thus be represented by a small number of wavelet coefficients. Previous studies by the authors on GUV defect detection in strands (Rizzo and Lanza di Scalea 2004b) demonstrated signal compression performances on the order of 99.7% after wavelet thresholding. In that study the defect-sensitive information of GUV signals, originally consisting of 9,000 points in the time domain, was reduced down to only 27 wavelet coefficients.

The DWT processing used in the present work adopted the Daubechies mother wavelet of order 40 (db40) due its similarity to the narrowband ultrasonic signals employed to probe the strands (Rizzo and Lanza di Scalea 2004b). In previous works (Lanza di Scalea, *et al.* 2003, Rizzo and Lanza di Scalea 2004a, b and 2005a) the authors found that 320 kHz is a low-loss frequency for the fundamental GUV mode propagating in typical loaded seven-wire strands (0.6 in diameter). The appropriate DWT level for pruning was chosen as the one that most closely represented the frequency band of interest following the known relation:

$$f_j = \Delta \times F / 2^j \quad (1)$$

relating the reconstructed frequency f_j at DWT level j , to the center frequency of the mother wavelet F , the scale 2^j and the signal sampling frequency Δ . For $\Delta = 33 \times 10^6$ Hz and $F = 0.671$ rad for the db40 wavelet, Eq. (1) yields $f_6 = 346$ kHz that is close to the low-loss signal frequency of 320 kHz that was used to excite the strands. Thus the sixth decomposition level was selected for all DWT-processed signals that follow.

3. Strand monitoring

3.1. Experimental setup

The experimental setup adopted was the same as in Rizzo and Lanza di Scalea (2005a), and it is described here for the sake of completeness. The test component was a high-grade steel 270, seven-wire twisted strand with a total diameter of 15.24 mm (0.6 in). This is a typical strand for stay cables and for prestressed concrete structures. The nominal diameter of each of the wires was 5.08 mm (0.2 in). A notch was machined in one of the six peripheral wires by saw-cutting with depths increasing by 0.5-mm steps to a maximum depth of 3 mm. A final cut resulted in the complete fracture of the helical wire (broken wire, b.w.), which was the largest defect examined. The notches were machined perpendicular to the strand axis. Fig. 1(a) illustrates the eight defect sizes monitored. Fig. 1(b) shows the cross-sectional area reductions corresponding to the various notch depths.

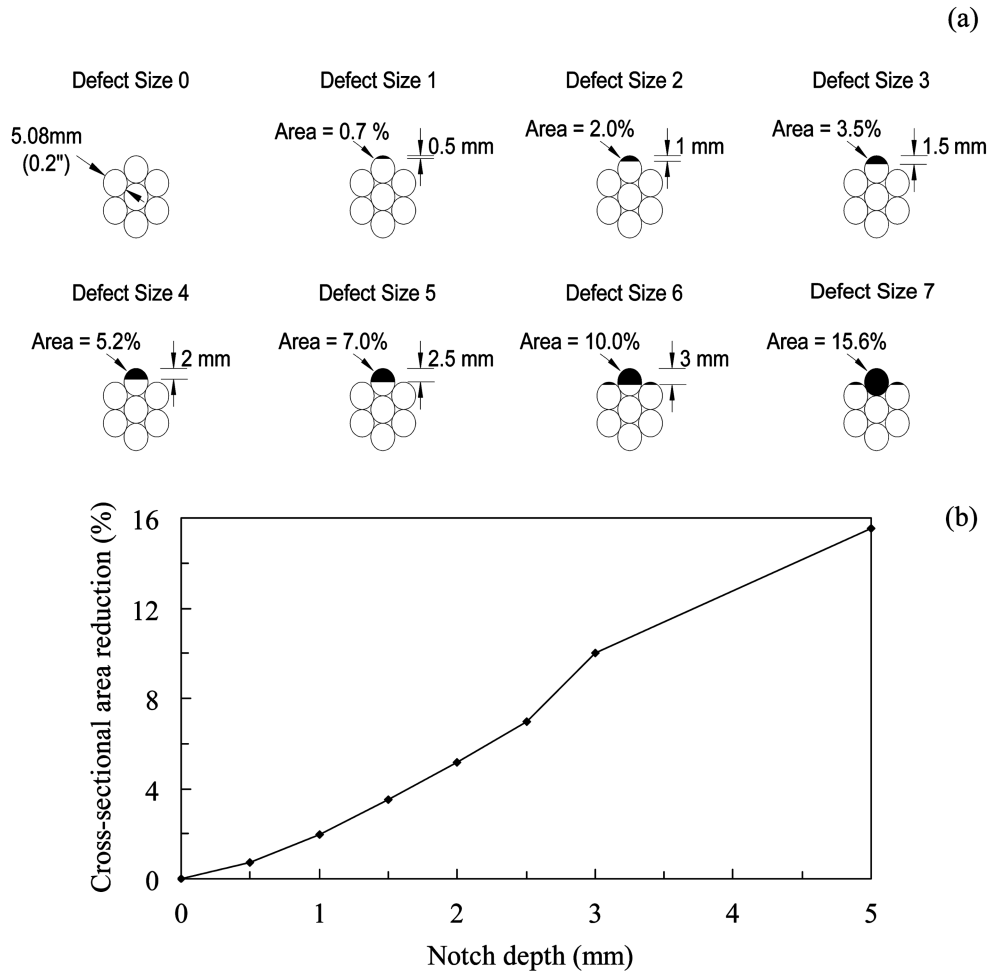


Fig. 1 (a) The different notch depths examined; (b) reduction of the cross-sectional area of the strand as a function of notch depth

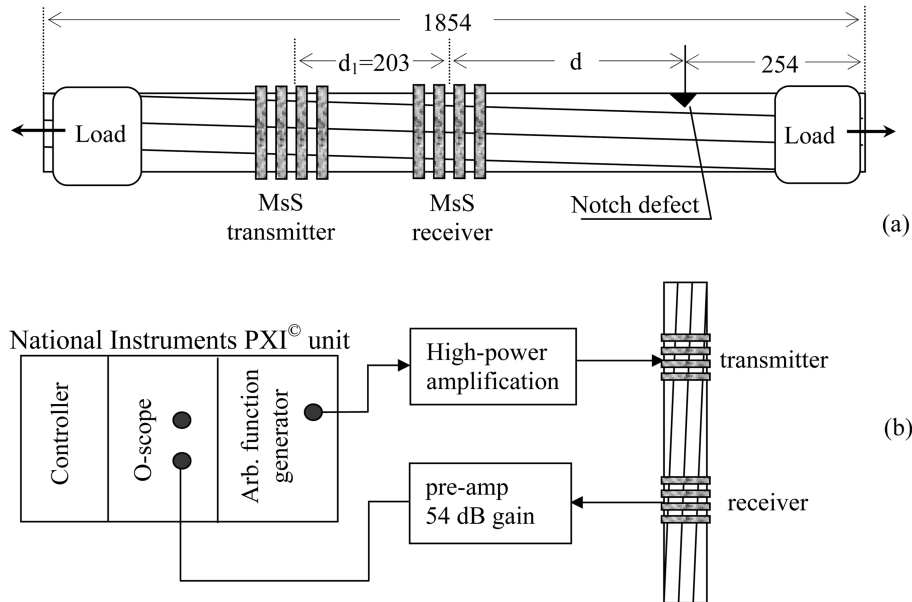


Fig. 2 (a) Experimental setup for the detection of notch defects in the strand (dimensions in mm); (b) overall schematic of the monitoring system

The strand was subjected to a 120 kN tensile load, corresponding to 45% of the material's ultimate tensile strength, that is a typical operating load for stay cables. The load was applied in the laboratory by a hydraulic jack.

Magnetostrictive sensors (MsS), resonant at 320 kHz, were used to excite and detect GUWs. This frequency was chosen since it is known to propagate with little losses in loaded strands as discussed above. The distance between the transmitting and the receiving transducers, d_1 in Fig. 2(a), was fixed at 203 mm (8 in) in all tests. By sliding the transmitter/receiver pair along the strand, tests were conducted at the five different notch-receiver distances, d in Fig. 2(a), of 203 mm (8 in), 406 mm (16 in), 812 mm (32 in), 1016 mm (40 in), and 1118 mm (44 in). The latter was the largest distance allowed by the rigid frame of the hydraulic loading.

A National Instruments PXI unit running under LabVIEW was employed for signal excitation, detection and acquisition, Fig. 2(b). Five-cycle tonebursts centered at 320 kHz, modulated with a triangular window, were used as generation signals. Signals were acquired at sampling rate equal to 33 MHz and stored after different number of digital averages, namely 500, 50, 10, 5, 2 and 1 (single generation). Table 1 summarizes the various testing configurations.

3.2. Damage index

An efficient damage index must be robust against noise and must allow for the detection, the sizing and the location of the defect. These performances were achieved by the appropriate selection of the signal features used for the damage index computation.

The Damage Index (D.I.) proposed in this study uses the ratio between certain features of the reflection from the defect, $F_{\text{reflection}}$, and the same features of the signal traveling directly from the transmitter to the receiver, F_{direct}

Table 1 The different testing configurations considered

Defect size (mm)	Strand cross-sectional area reduction (%)	Notch-receiver distance d (mm)	Number of averages on GUV signals
0	0.00	203	1
0.5	0.71	406	2
1	1.98	812	5
1.5	3.50	1016	10
2	5.18	1118	50
2.5	6.97		500
3	10.0		
Broken wire	15.6		

$$D.I. = \frac{F_{\text{reflection}}}{F_{\text{direct}}} \quad (2)$$

Normalizing the defect reflection by the direct signal eliminates any dependence of the monitoring result on the generation signal power or on the transducer/strand electro-mechanical coupling efficiency. The concept is analogous to considering reflection coefficients for detecting defects in ultrasonic NDE. If a defect is a perfect reflector of the ultrasonic energy, the D.I. is 1. For the notch defects examined in this study, the D.I. will be smaller than one since only a small portion of the incoming signal will be reflected.

The same expression for the D.I. was adopted by Rizzo and Lanza di Scalea (2005b), although that study used only a subset of the features examined in the present work and it did not consider any pattern recognition analysis.

The selection of the signal features for the computation of the D.I. is the most critical task. Optimum features are those allowing for quantitative defect detection with the smallest possible number of signal averages. Initially, features were extracted in the time domain (peak-to-peak and variance), in the frequency domain (peak of Fast-Fourier Transform - FFT amplitude spectrum at propagating frequency), and in the joint time-frequency domain (variance of reconstruction after DWT pruning). The variance is a known features for structural monitoring (Staszewski, *et al.* 2004), and is defined by the well known relations:

$$\text{variance} = \frac{1}{N-1} \sum_{i=1}^N (x_i - \bar{x})^2$$

where \bar{x} represents the mean value of the collection of N data points. The variance can be interpreted as the variability of the signal from the mean.

3.3. Feature selection

Two time windows were selected for the direct signal and the defect reflection. The direct signal window was fixed between 35 μsec and 97 μsec for the given constant transmitter-receiver distance and it consisted of 2048 points, Figs. 3(a) and (b). The defect reflection window varied for the different notch-receiver distances. Such window consisted of 4096 points, Figs. 3(c) and (d), and covered the expected arrival of the reflection considering a wave velocity for the lowest-order longitudinal

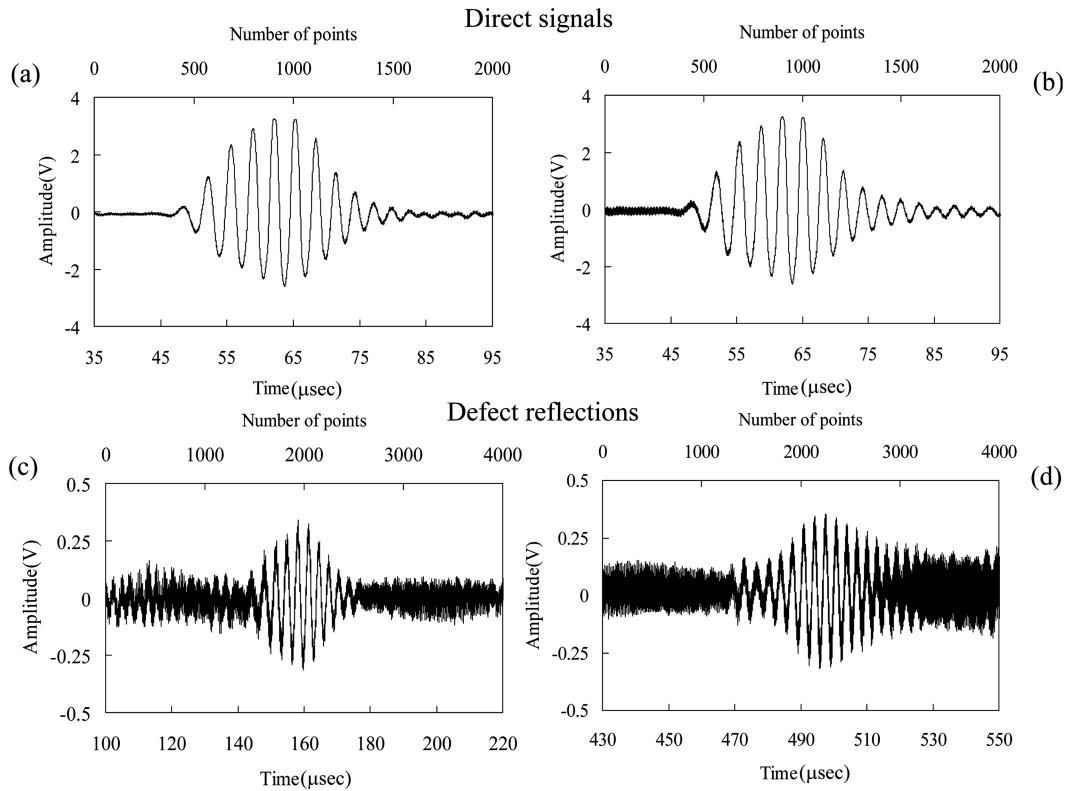


Fig. 3 Probing the 3 mm-deep notch. Direct signal with (a) notch-receiver distance $d=203$ mm and (b) $d=1016$ mm. Defect reflection with (c) $d=203$ mm and (d) $d=1016$ mm. Signals stored after 500 averages

dominant mode at 320 kHz. The signals shown in Fig. 3 refer to the case of the 3 mm notch depth, after 500 signal averaging. Particularly, Figs. 3(a) and (c) are relative to the notch-receiver distance $d=203$ mm, while Figs. 3(b) and (d) are relative to the case of $d=1016$ mm. Notice the poorer SNR of the defect reflection for the larger distance of Fig. 3(d) compared to Fig. 3(c).

The performance of the four initial features used to compute the D.I. is illustrated in Fig. 4. For clarity, this figure shows only the results for notch depths at 1-mm increments (four damage scenarios), for all six different numbers of averages (1 i.e. single-generation, 2, 5, 10, 50 and 500). The zero notch depth is the “no defect” case. The notch-receiver distance was 1,016 mm. The values of the D.I. are plotted in a logarithmic scale. The desirable properties of the D.I. are stability against number of averages and linear, monotonic increase with increasing notch depth for ease of defect sizing. The rate of change of the D.I. with notch depth (slope of connected points in Fig. 4) can be viewed as the sensitivity to damage size.

The D.I. computed with the time-domain peak-to-peak ratio, Fig. 4(a), shows a large dependence on the number of averages. This implies that the peak-to-peak feature is not robust against noise. At least 50 averages are needed in this case to obtain a D.I. that is monotonically increasing with defect size. The time-domain variance, Fig. 4(b), shows the same drawbacks of unstable results. The only improvement over the peak-to-peak feature is an increase in defect sizing sensitivity (slope of the connected points) but, again, only once at least 50 averages are used to obtain a monotonic trend. The variance performs

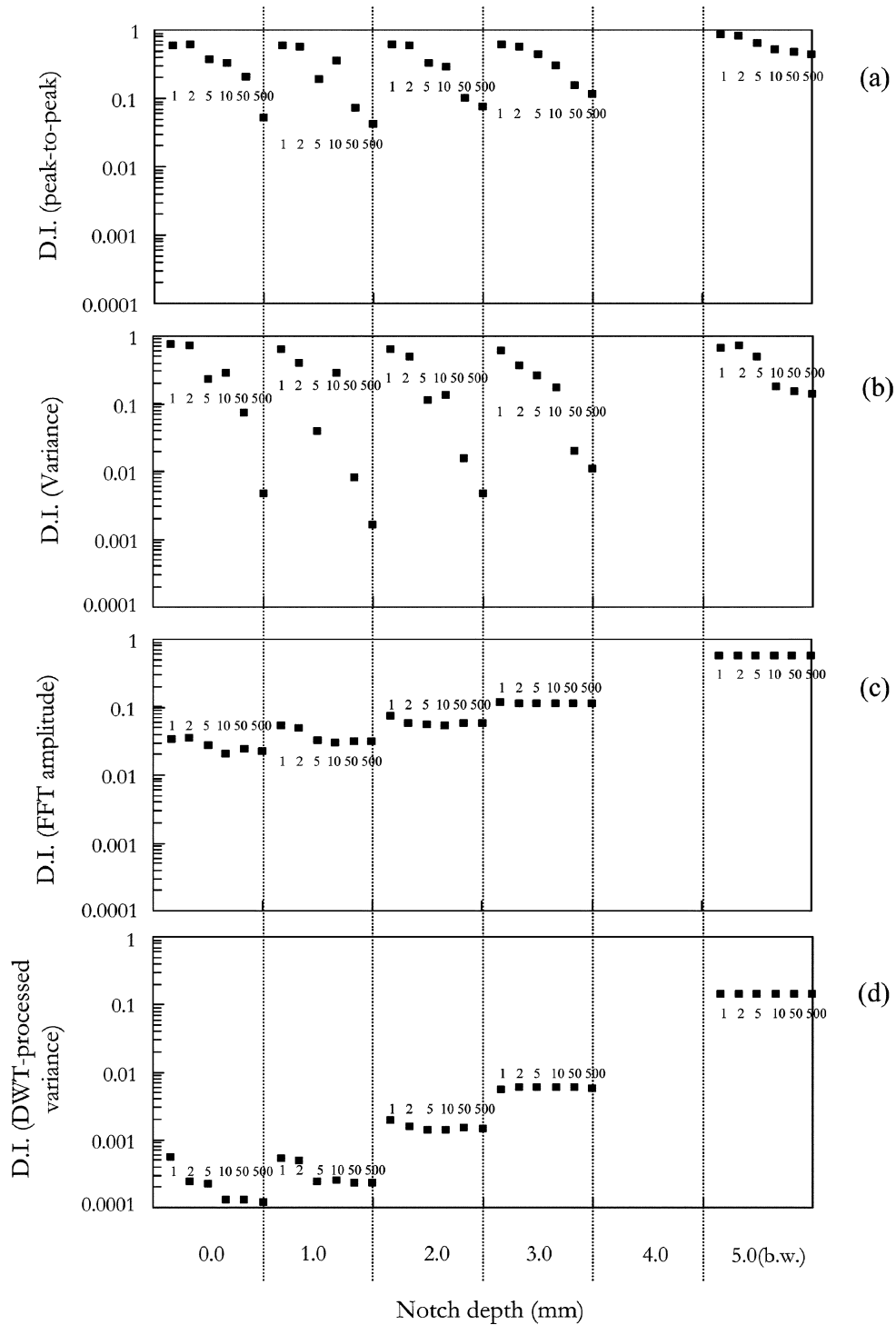


Fig. 4 Damage index computed for varying notch depths and varying number of averages considering (a) the time-domain peak-to-peak, (b) the time-domain variance, (c) the FFT peak amplitude, and (d) the variance of the reconstruction after DWT pruning and thresholding

slightly better than the peak-to-peak because it accounts for the entire signal waveform, rather than just its extreme values.

When the frequency-domain feature of FFT amplitude is used, Fig. 4(c), substantial improvements are found. The D.I. is now extremely stable against number of averages for notches deeper than 2 mm. For very small notches, below 2 mm, as few as 5 averages are needed to obtain a stable result. In the frequency domain noise is partially filtered out, hence the better result than the previous two cases.

Further improvements are obtained if the variance feature is extracted after DWT processing, Fig. 4(d). In terms of number of averages, the DWT-processed variance is as stable as the FFT peak. However, a large increase in defect sizing sensitivity can be seen by an increased slope of the D.I. data in Fig. 4(d). In fact, the sensitivity of the DWT-processed variance is doubled compared to that of the FFT peak. This result proves that the DWT processing performs a better de-noising than the conventional frequency-domain filtering and it thus detects better the defect signatures. The reason is that broadband noise always affects the features extracted in the frequency domain. The unmatched de-noising performance of the DWT is also such that as few as 5 averages are needed to yield the same D.I. as 500 averages for notches as shallow as 1 mm. This represents a large gain in computational efforts and speed of the inspection. Also, de-noising allows for a reduced power to the transmitting sensors that would be a desirable feature in any field implementation of the technique.

3.4. Wavelet coefficient analysis

It was shown that the analysis of the signals reconstructed after DWT pruning offers a reliable tool for damage sizing. Damage-related features can be also computed directly on the wavelet coefficients before signal reconstruction takes place. This method eliminates half of the DWT processing task. The statistical features of the root mean square (RMS), the variance, the kurtosis, the peak amplitude, and the peak-to-peak value of the wavelet coefficients were examined as features for the D.I. in this portion of the study. The RMS and the kurtosis are defined by the classical expressions:

$$\text{RMS} = \sqrt{\frac{\sum_{i=1}^N x_i^2}{N}} \quad (4)$$

$$\text{Kurtosis} = \frac{\sum_{i=1}^N (x_i - \bar{x})^4}{\text{RMS}^4} \quad (5)$$

The decomposition of a typical ultrasonic time waveform into wavelet coefficients is illustrated in Fig. 5, showing the direct signal (Fig. 5a) and the defect reflection (Fig. 5b) for the 2 mm-deep notch, at a notch-receiver distance of 203 mm. These results were taken after 50 averages. Notice that the scale amplitude of the reflection is set to one order of magnitude smaller than that of the direct signal. The vectors of the wavelet coefficients at level 6, cD_6 , are shown in Figs. 5(c) and 5(d), respectively. Since the number of points of the original signals differs (2048 for the direct signal and 4096 for the defect reflection), the size of the two wavelet coefficient vectors differs as well (109 versus 141).

It should be noted that most of the wavelet coefficients in Figs. 5(c) and 5(d) have very low amplitude and thus do not carry any information on the signal of interest. These can be eliminated by setting a threshold equal to 20% of the maximum coefficient amplitude. The thresholded coefficient vectors are

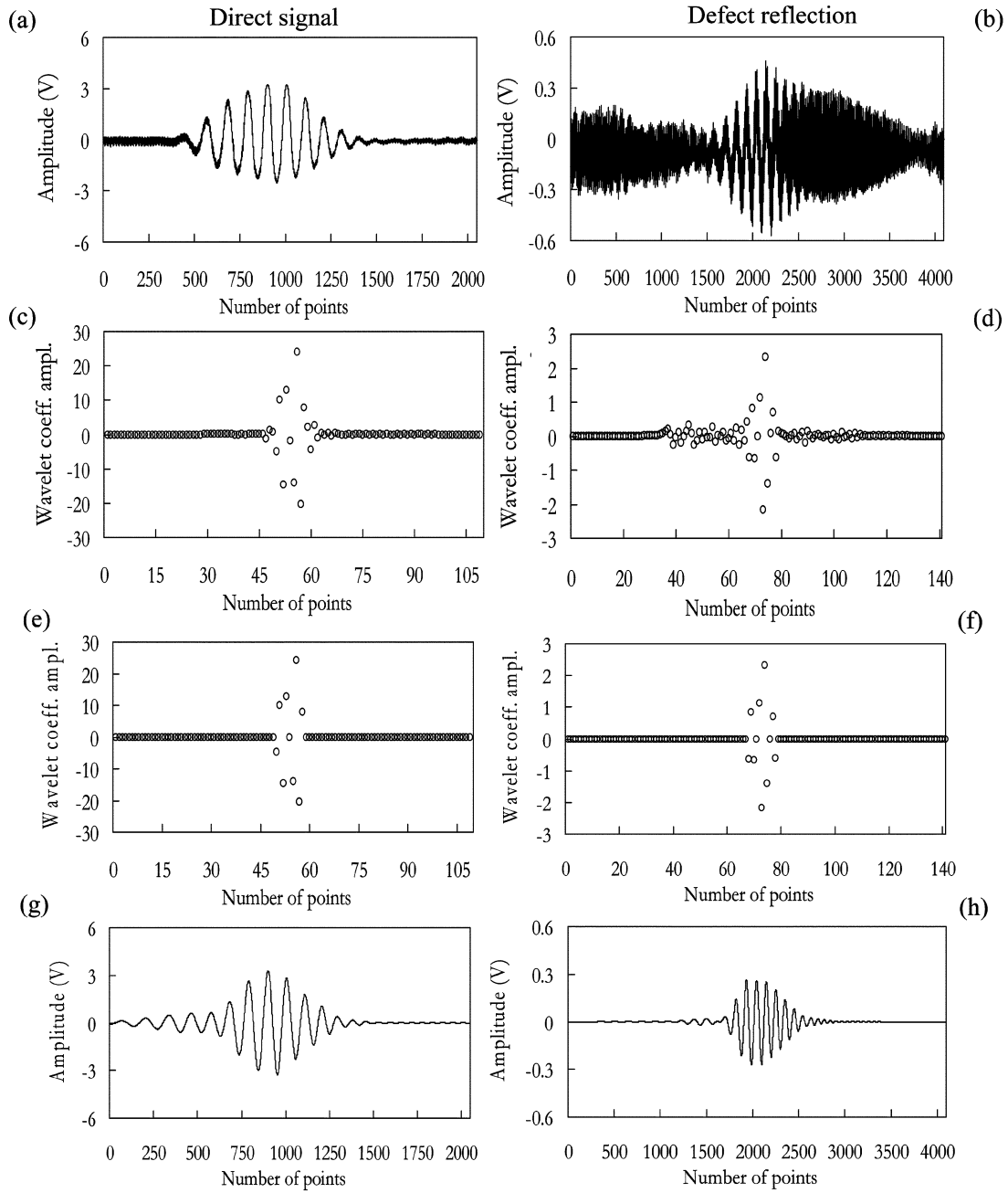


Fig. 5 (a) Direct signal; (b) reflection from 2 mm-deep notch 203 mm away from receiver; (c) wavelet coefficient vector cD_6 for direct signal; (d) wavelet coefficient vector cD_6 for defect reflection; (e) wavelet coefficient vector cD_6 for direct signal after 20% thresholding; (f) wavelet coefficient vector cD_6 for defect reflection after 20% thresholding; (g) reconstructed direct signal; (h) reconstructed defect reflection

shown in Figs. 5(e) and (f) for the direct signal and the defect reflection, respectively. Finally, the signals reconstructed from these vectors are shown in Figs. 5(g) and (h) and they demonstrate that the

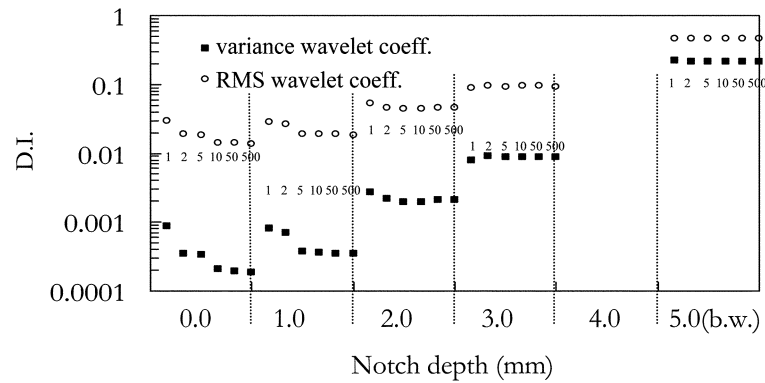


Fig. 6 Damage index computed from the variance and the RMS of wavelet coefficient vectors cD_6 for direct signal and for defect reflection after 20% thresholding

few thresholded wavelet coefficients indeed represent the information of interest. By considering only the relevant wavelet coefficients, the D.I. is very robust against noise.

The D.I. results are shown in Fig. 6 in terms of variance and RMS of the 20% thresholded wavelet coefficients of cD_6 . These results are for notch-receiver distance of 1,016 mm. It can be seen that the variance results computed directly on the wavelet coefficients match those in Fig. 4(d) that were computed on the signal reconstructions. The RMS results show the same trend, although their sensitivity to damage size (slope of the connected points) is reduced when compared to the variance analysis. This is a direct result of the square relationship between these two features.

3.5. Effect of wavelet threshold level

The threshold chosen to select the relevant wavelet coefficients for the D.I. computation is an important variable that affects the sensitivity of the defect sizing. The 20% threshold used in the previous section was chosen based on simple visual observation of the wavelet coefficient vector cD_6 . In a recent study, Rizzo and Lanza di Scalea (2005b) carried out a parametric study to find an optimum threshold combination for the direct signal and the defect reflection, respectively. The optimum combination was defined as the one resulting into the largest sensitivity to defect size of the variance-based D.I. It was found that the larger sensitivities are obtained when setting more severe thresholds to the defect-reflected signals, with little effect of the threshold to the direct signal. Thus parametric studies to determine optimum threshold values need only to be conducted on the defect reflections, that are the most delicate element of the D.I. computation because of the poorer SNRs associated to the small defects of interest in this study. Based on the findings in Rizzo and Lanza di Scalea (2005b), optimum thresholds were identified at 20% for the direct signal and at 70% for the defect reflection. These values were used for the analysis of the results that follow.

3.6. Damage index vector

DIs based on the variance, the RMS, the kurtosis, the peak amplitude and the peak-to-peak amplitude of the thresholded wavelet coefficient vectors were evaluated. The direct signals and the defect reflections were then reconstructed from the wavelet coefficient vectors. The following features were

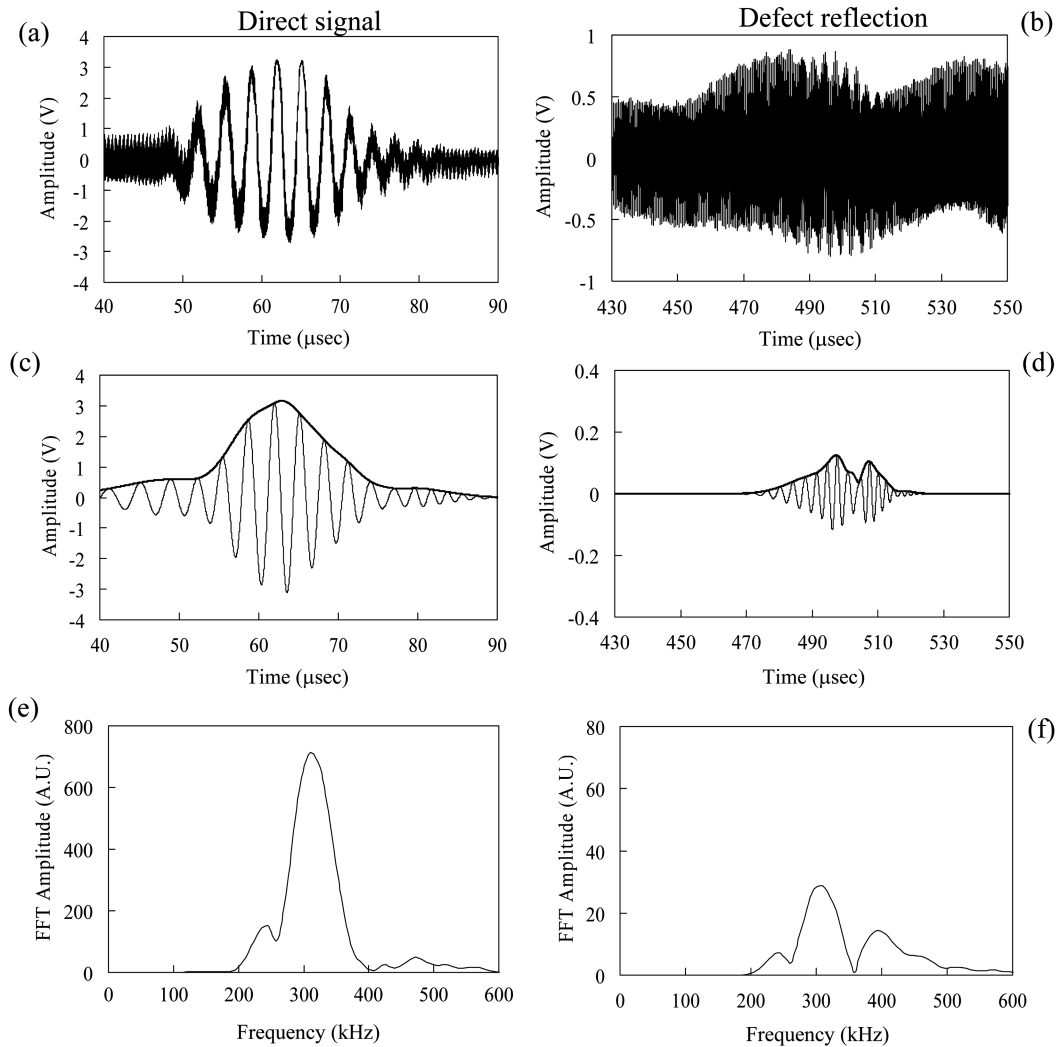


Fig. 7 Raw time waveforms of (a) the direct signal, and (b) the reflection from a 1.5 mm-deep notch located 1,018 mm from the receiver; reconstructed waveforms and Hilbert transform envelopes of (c) the direct signal, and (d) the defect reflection; (e) FFT amplitude of (c); (f) FFT amplitude of (d)

extracted from the reconstructed signals: the position and the magnitude of the Hilbert transform peak, the area below the Hilbert transform, the peak amplitude of the FFT spectrum, and the area below the FFT spectrum. All features considered except one were related to the *size* of the defect. The one exception was the position of the Hilbert transform peak that made the D.I. dependent on the *location* of the defect, in addition to the size. In fact, the Hilbert transform peak position corresponds to the arrival time of the waves, in turn related to the defect location through the wave velocity.

Figs. 7(a) and (b) show the raw signals stored after 10 averages for the 1.5 mm-deep notch, with a notch-receiver distance $d = 1018$ mm. The corresponding reconstructed signals (20%-70% threshold combination) are shown in Figs. 7(c) and (d) together with the curve-envelope from the Hilbert transform. The FFT amplitude spectra of the reconstructed signals are presented in Figs. 7(e) and (f).

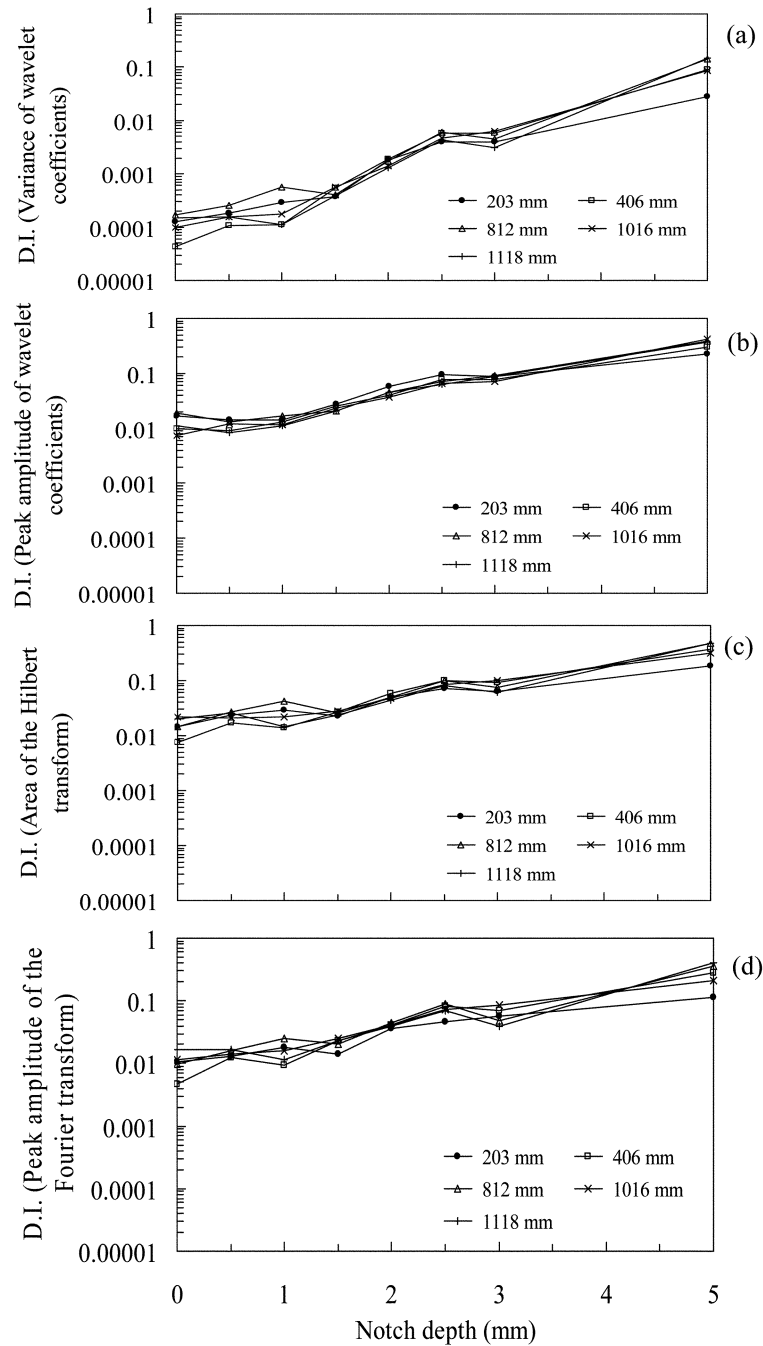


Fig. 8 Unidimensional damage indices for varying notch depths and notch-receiver distances considering (a) the variance of the wavelet coefficients, (b) the peak amplitude of the wavelet coefficients, (c) the area of the Hilbert Transform of the reconstructions, and (d) the FFT peak amplitude of the reconstructions

The unidimensional D.I.s computed using some of the individual features are shown in Fig. 8 as a function of the notch depth and notch-receiver distance. The results were computed after 10 averages.

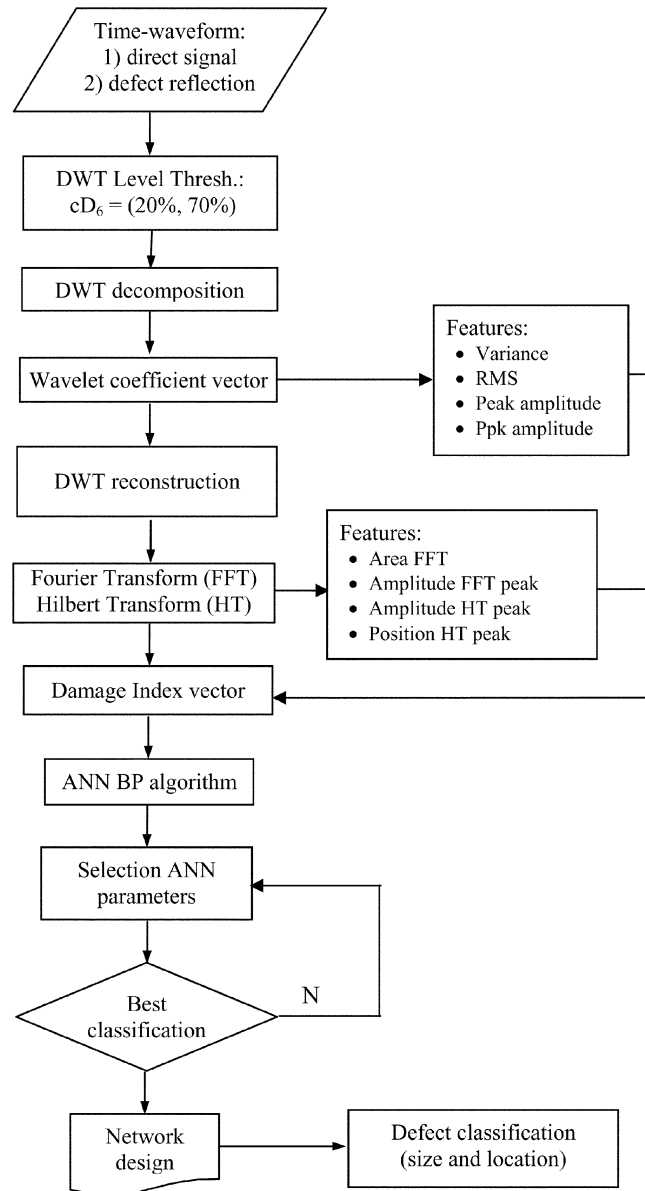


Fig. 9 Flowchart of the proposed strategy for classifying the size and the location of defects in strands by guided ultrasonic waves

The D.I.s shown are based on the variance and the peak amplitude of the wavelet coefficients (Figs. 8a and b), on the area below the Hilbert transform (Fig. 8c), and on the peak amplitude of the FFT spectrum (Fig. 8d). All D.I.s show a quite linear dependence in logarithmic scale on the notch depth, and a relatively negligible dependence on the defect position for notches between 1.5 mm and 3 mm in depth. The results for very small notches, below 1 mm in depth, are less stable against varying distances due to the poorer SNRs of the defect reflections. The results for the broken wire case (5mm-deep notch)

also show an increased dependence on the notch-receiver distance, with D.I.s generally increasing for defects located further away from the receiver. This trend is opposite to what would be expected considering wave attenuation effects, and its origins are still under investigation. One possibility is the interference of multiple propagating modes that is distance dependent. One of the most clear results in Fig. 8 is that the D.I. based on the variance of the wavelet coefficient vector, Fig. 8(a), has the largest sensitivity on notch depth compared to the other features presented.

Of the total ten DWT-processed features discussed above, eight were used to assemble a multi-dimensional D.I. vector for the ANN classification. The two discarded features were the kurtosis of the wavelet coefficients and the Hilbert transform area of the reconstructions. The choice of features to consider for the ANN was based on the behavior of the unidimensional D.I.s of the type shown in Fig. 8. The general defect classification strategy is illustrated in the flowchart of Fig. 9. The next section presents the last step of this strategy that is the pattern recognition.

4. Automatic defect classification

Table 2 summarizes the definition of the classes considered in the pattern recognition algorithm. The defect sizes were subdivided into four classes (Classes 1, 2, 3 and 4), corresponding to strand's area reductions in the ranges 0% - 1%, 2% - 5%, 7% - 10%, and 16%. Class 1 can be considered the "no defect" case. Similarly, the notch-receiver distances were subdivided into four classes (Classes A, B, C

Table 2(a) Defect classification problem definition

Class	Defect size (mm)	Strand area reduction (%)	Binary code	Notch-receiver distance (mm)	Binary code
1	0 – 0.5	0 – 1	0 0		
2	1 – 2	2 – 5	0 1		
3	2.5 – 3	7 – 10	1 0		
4	Broken wire	16	1 1		
A				203	0 0
B				406	0 1
C				812	1 0
D				1018-1116	1 1

Table 2(b) Coding for the classification problem

Combination	Binary code	Combination	Binary code
1A	0 0 0 0	3A	1 0 0 0
1B	0 0 0 1	3B	1 0 0 1
1C	0 0 1 0	3C	1 0 1 0
1D	0 0 1 1	3D	1 0 1 1
2A	0 1 0 0	4A	1 1 0 0
2B	0 1 0 1	4B	1 1 0 1
2C	0 1 1 0	4C	1 1 1 0
2D	0 1 1 1	4D	1 1 1 1

and D) corresponding to the values $d = 203$ mm, 406 mm, 812 mm and 1016-1118 mm. Each class of defect size and notch-receiver distance was coded with a 2-digit binary number. In total, the classification problem consisted of $4^2 = 16$ combinations of defect sizes and notch-receiver distances, represented by the four digit codes shown in Table 2(b).

A feed-forward, backpropagation ANN with three layers was used as the algorithm. The input layer receives as input data the multi-dimensional D.I. vectors along with the codifications of their classes (targets). The hidden layer processes the data by multiplying the input vectors by weights and adding biases. The results constitute the argument of a transfer function that squashes the output values into a certain range. Since the target classes were coded with binary numbers, the following log-sigmoid transfer function was employed

$$f(x) = \frac{1}{1 + e^{-x}} \quad (6)$$

This function squashes the output values between zero and one for the binary representation. The output layer provides the network outputs and compares the outputs with the targets. The error E is calculated as

$$E = \frac{1}{N} \sum_{k=1}^N \sum_{j=1}^m (y_{kj} - \hat{y}_{kj})^2 \quad (7)$$

where N is the number of training samples (40 D.I. vectors in the present case), m is the number of output nodes (number of elements that code the classes, 4 in the present case), y_{kj} is the desired target, and \hat{y}_{kj} is the network output. If the error is above a certain value, the training process is continued by transmitting the errors backwards from the output layers, and adjusting the weight and biases. If the error is below an established value, the learning process is stopped. The training process is also stopped when a minimum on the error gradient is reached. Each individual weight change is in the direction of a negative gradient and at the iteration step, n , the new weight vector is

$$\underline{w}(n+1) = \underline{w}(n) - \eta \frac{\partial E}{\partial w_{jp}} \quad (j=1, \dots, m; p=1, \dots, \# \text{ of features}) \quad (8)$$

where $0 < \eta < 1$ is the learning rate. The learning rate determines the magnitudes of the weight change. The smaller η , the smoother the convergence of the search at the price of a higher number of iteration steps. For higher values of η , the algorithm may become unstable possibly leading to oscillations and preventing the error to fall below a certain range. In order to control the network oscillations during the training process, an additional coefficient η_m (momentum coefficient or additional momentum), comprised between 0 and 1, was added to the definition in Eq. (8). The weight change now becomes:

$$\underline{w}(n+1) = \underline{w}(n) - \eta \frac{\partial E}{\partial w_{jp}} - \eta_m [\underline{w}(n) - \underline{w}(n-1)] \quad (9)$$

The additional coefficient scales the influences of the previous step on the current one.

Eight (defect sizes) \times five (notch-receiver distances) = 40 D.I. vectors used as training data in the present analysis corresponded to all acquisitions after 500 averages. This was considered to be a representative baseline configuration. The training data represented the 16.7% (1/6) of all the data measured.

A few parameter analyses were conducted in order to find the design that provided the best network performance, i.e., the largest percentage of testing data correctly classified. A summary of the parameters

Table 3 Network parameters considered

Feature #	D.I. feature	η = learning rate	η_m = additional momentum	# of features	# of hidden neurons
1	Variance (WCV)	0.05	0.05	3 to 8	6 to 20
2	Peak position (HT)	0.20	0.20	step 1	step 2
3	Peak-to-peak (WCV)	0.35	0.35		
4	Peak amplitude (HT)	0.50	0.50		
5	Peak amplitude (FFT)	0.65	0.65		
6	RMS (WCV)	0.80	0.80		
7	Peak amplitude (WCV)	0.95	0.95		
8	Area (FFT)				

WCV: wavelet coefficient vector

HT: Hilbert Transform

FFT: Fast-Fourier Transform

considered for this optimization is presented in Table 3. In order to ensure the same initial conditions, the initial biases and weights of the network were constrained to be constant.

The first analysis considered the values of the learning rate, η , and the additional momentum, η_m , as parameters, columns 3 and 4 in Table 3. The network consisted of eight hidden neurons with eight-dimensional input vectors. The input vector consisted of the D.I. based upon the eight features listed and ordered in columns 1 and 2 of Table 3. The analysis demonstrated that for this application the two parameters η and η_m did not substantially affect the performance of the network.

The second analysis considered fixed values for η (= 0.2) and η_m (= 0.5). The goal now was to find the *best* network configuration by selecting the parameters resulting in the best classification performance in terms of (a) the number of features (dimension) of the input D.I. vector, (b) the type of these features, and (c) the number of hidden neurons. The first two features of the D.I. vector were kept constant in the optimization process. These were the variance of the wavelet coefficients (providing the highest sensitivity to the notch size) and the position of the Hilbert transform peak of the reconstructions (providing the sensitivity to the notch location). The analysis then proceeded by adding the remaining six features of Table 3 to the D.I. vector, one at a time and in all possible combinations. Thus D.I. vectors were tested from a minimum of three dimensions to a maximum of eight dimensions. For each input vector, the number of hidden neurons was changed from 6 to 20. This extensive set of trials resulted in a network performance varying between 41.2% for the *worst* network (5-dimensional D.I. input vector, features 1, 2, 3, 6, 8 in Table 3, with 6 hidden neurons) and 90.8% for the *best* network (5-dimensional D.I. input vector, features 1, 2, 4, 5, 6 in Table 3, and 12 hidden neurons).

The histograms in Fig. 10 summarize the performance of the *best* network design. The percentage of correct classification is plotted as a function of various testing parameters. Fig. 10(a) shows the classification performance for varying notch sizes. The best performance is obtained for the two largest defects, above 7% of the strand area reduction. These notches were all properly identified as a result of the large SNR of the reflections. The poorest performance is obtained for the “no defect” case, but still with a success rate as high as 82%. Properly classifying the “no defect” case means avoiding false positives.

The histograms in Figs. 10(b) and (c) can be read in a similar way. They are plotted by clustering the number of averages (Fig. 10b) and the notch-receiver distances (Fig. 10c). Fig. 10(b) shows the

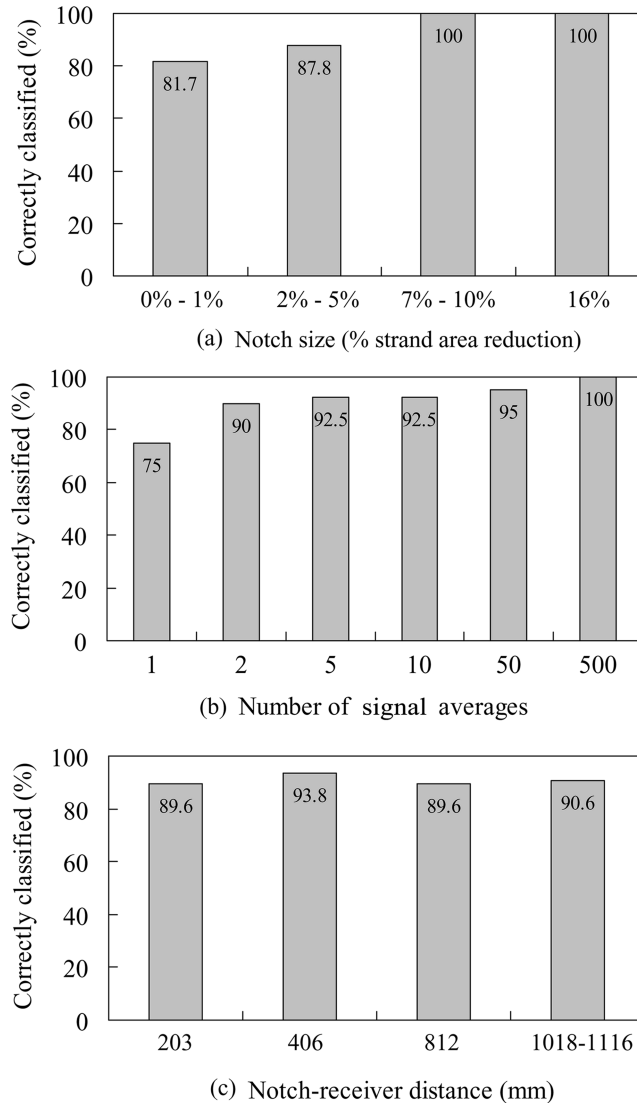


Fig. 10 Best defect classification performance of the 16-combination problem as function

interesting result that the classification performance is rather independent of the number of averages. This confirms what seen in Fig. 4, and remarks the fact that the DWT-based features chosen for the D.I. vector computation are robust against noise. The classification success is naturally poorer (75%) for the single-event case due to the degraded SNR. Similarly, the classification performance appears substantially independent of the notch-receiver distance, Fig. 10(c).

In the *best* network only 9.2% of the cases (22 testing data) were not properly classified. These included false positives (2.9%), false negatives (3.7%), misclassifications (0.8%) and undetermined outputs (1.7%). The 3.7% false negative indications, the most critical in structural monitoring, were nine cases of Class 2 notch sizes incorrectly classified in the “no defect” Class 1. These “missed” defects corresponded to a 2% reduction of the strand’s cross-sectional area, thus very small.

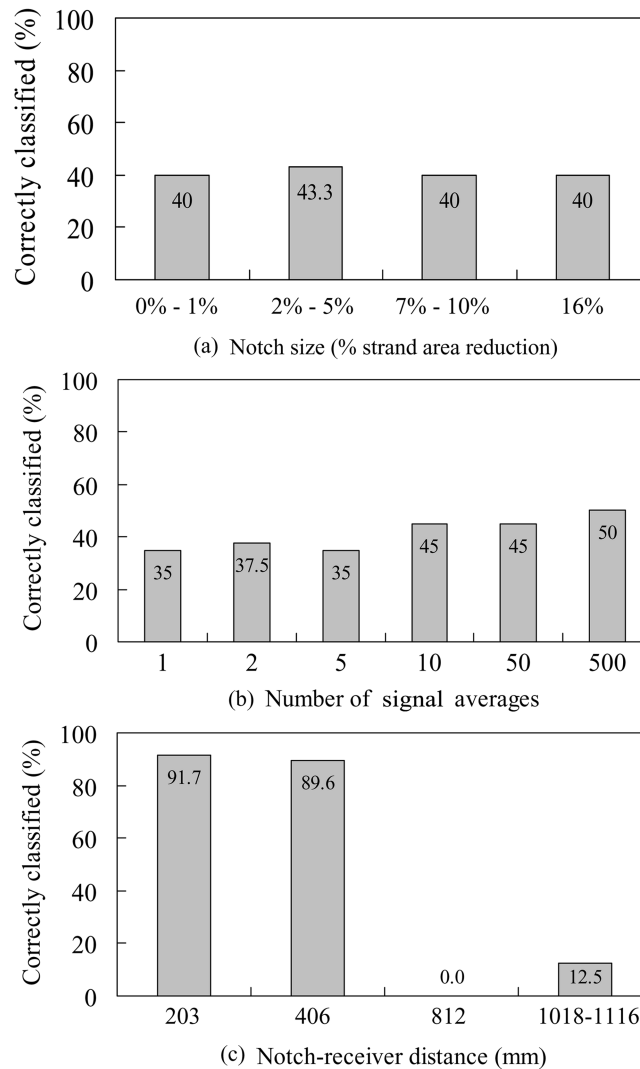


Fig. 11 Worst defect classification performance of the 16-combination problem as function

The performance of the *worst* network design (features 1, 2, 3, 6, 8, and 6 hidden neurons) is reported for comparison in the histograms of Fig. 11. It is clear that the classification rates of success are poorer than those in Fig. 10. The only result that is comparable between the *worst* and the *best* networks is the classification of the defect location, and only for the notches that are closer to the receiver. In the *worst* network, even the training data used in the testing phase were properly classified in only 50% of the cases.

5. Summary and conclusions

Improvements to the technique based on Guided Ultrasonic Waves for the structural monitoring of strands were proposed in terms of defect-sensitive feature extraction and defect classification. The

goal was to determine the size and the location of notch-like defects based on ultrasonic reflection measurements.

Notches were machined in one of the six helical wires of a seven-wire strand, loaded to 45% U.T.S. The defects resulted in incremental reductions of the strand's cross-sectional area up to a maximum of 15.6% corresponding to a completely broken wire. The notches were probed by low-loss ultrasonic signals at 320 kHz, that were excited and detected by a pair of magnetostrictive ultrasonic transducers.

Based on eight features extracted after DWT processing, a multi-dimensional Damage Index vector was fed into an Artificial Neural Network. A parametric study was conducted to optimize the architecture of the network. The study identified the best combination of features for assembling the Damage Index vector. The best vector contained five features, four of which related to the *size* of the defect and one, the Hilbert transform peak position, to the *location* of the defect. The optimized network had an overall success rate of classification (defect size and location) of 90.8% among 240 different acquisitions at varying defect sizes, locations and number of averages. Within the incorrect classifications, the dangerous false negatives (missed defects) accounted for only 3.7% of the total cases examined. These false negatives were recorded for a small subset of data from notches as small as 2% of the strand's cross-sectional area, and thus constituted an acceptable margin of error.

The maximum notch-receiver distance examined in this study was 1,118 mm. Therefore the effectiveness of the proposed technique remains localized to a limited portion of the strand. One portion of stay-cable or post-tensioning strands that does not require large monitoring ranges is the anchored end, that is particularly prone to corrosion and stress concentrations due to the restraining wedges. Arrays of magnetostrictive transducers located at fixed intervals must be used if coverage of the entire cable is required.

For defects located further away from the sensors, the thresholds imposed to the wavelet coefficients will most likely have to change, and the best combination of the damage-sensitive features may also change. The same defect classification strategy is being applied to grouted, rather than free strands. In grouted strands the ultrasonic attenuation losses will be higher and the overall defect classification performance of the method will be reassessed.

Acknowledgements

This research was supported by the National Science Foundation grant CMS-0221707. Mr. Ivan Bartoli at UC San Diego is acknowledged for preparing Fig. 1(a).

References

- Abbate, A., Koay J., Frankel, J., Schroeder, S. C. and Das, P. (1994), "Application of wavelet transform signal processor to ultrasound", *Proc. 1994 Ultrasonic Symposium*, Vol. 94CH3468-6, 1147-1152.
- Abbate, A., Koay, J., Frankel, J., Schroeder, S. C. and Das, P. (1997), "Signal detection and noise suppression using a wavelet transform signal processor: application to ultrasonic flaw detection", *IEEE Transactions on Ultrasonic, Ferroelectrics, and Frequency Control*, **44**(1), 14-26.
- Beard, M. D., Lowe, M. J. S. and Cawley, P. (2003), "Ultrasonic guided waves for inspection of grouted tendons and bolts", *J. Mater. Civ. Eng.*, ASCE, **15**, 212-218.
- Chase, S. B. (2001), "Smarter bridges, why and how?", *Smart Materials Bulletin*, **2**, 9-13.

- Chen, H-L. and Wissawapaisal, K. (2001), "Measurement of tensile forces in a seven-wire prestressing strand using stress waves", *J. Eng. Mech.*, ASCE, **127**, 599-606.
- Chen, H-L. and Wissawapaisal, K. (2002), "Application of Wigner-Ville transform to evaluate tensile forces in seven-wire prestressing strands", *J. Eng. Mech.*, ASCE, **128**, 1206-1214.
- Kim, H. and Melhem, H. (2004), "Damage detection of structures by wavelet analysis", *Eng. Struct.*, **26**(3), 347-362.
- Kwun, H. and Teller, C. M. (1994), "Detection of fractured wires in steel cables using magnetostrictive sensors", *Materials Evaluation*, **52**, 503-507.
- Kwun, H. and Teller, C. M. (1995), "Nondestructive evaluation of steel cables and ropes using magnetostrictively induced ultrasonic waves and magnetostrictively detected acoustic emissions", U.S. Patent No. 5,456,113.
- Kwun, H., Bartels, K. A. and Hanley, J. J. (1998), "Effect of tensile loading on the properties of elastic-wave propagation in a strand", *J. the Acoustical Society of America*, **103**, 3370-3375.
- Lanza di Scalea, F., Rizzo, P. and Seible, F. (2003), "Stress measurement and defect detection in steel strands by guided stress waves", *J. Mater. Civil Eng.*, ASCE, **15**, 219-227.
- Mallat S. G. (1999), *A Wavelet Tour of Signal Processing*, Academic Press, New York, NY.
- McNamara, J. and Lanza di Scalea, F. (2004), "Improvements in non-contact ultrasonic testing of rails by the discrete wavelet transform", *Materials Evaluation*, **62**, 365-372.
- Na, W. B. and Kundu, T. (2002), "A combination of PZT and EMAT transducers for interface inspection", *J. the Acoustical Society of America*, **111**, 2128-2139.
- Na, W. B., Kundu, T. and Ehsani, M. (2003), "Lamb waves for detecting delamination between steel bars and concrete", *Computer-Aided Civil and Infrastructure Engineering*, **18**, 57-62.
- Paget, C. A., Grondel, S., Levin, K. and Delebarre, C. (2003), "Damage assessment in composites by Lamb waves and wavelet coefficients", *Smart Mater. Struct.*, **12**, 393-402.
- Parker, D. (1996a), "Pacific bridge collapse throws up doubt on repair method", *New Civil Engineer*, 12/12/96 and 12/26/96, 3-4.
- Parker, D. (1996b), "Tropical overload", *New Civil Engineer*, 10/17/96, 18-21.
- Pavlakovic, B. N., Lowe, M. J. S. and Cawley, P. (1999), "The inspection of tendons in post-tensioned concrete using guided ultrasonic waves", *Insight*, **41**, 446-452.
- Pavlakovic, B. N., Lowe, M. J. S. and Cawley, P. (2001), "High-frequency low-loss ultrasonic modes in imbedded bars", *J. Appl. Mech.*, ASME, **68**, 67-75.
- Rizzo, P. and Lanza di Scalea, F. (2001), "Acoustic emission monitoring of carbon-fiber-reinforced-polymer bridge stay cables in large-scale testing", *Experimental Mechanics*, **41**, 282-290.
- Rizzo, P. and Lanza di Scalea, F. (2004a), "Wave propagation in multi-wire strands by wavelet-based laser ultrasound", *Experimental Mechanics*, **44**, 407-415.
- Rizzo, P. and Lanza di Scalea, F. (2004b), "Load measurement and health monitoring in cable stays via guided wave magnetostrictive ultrasonics", *Materials Evaluation*, **62**, 1057-1065.
- Rizzo, P. and Lanza di Scalea, F. (2005a), "Ultrasonic inspection of multi-wire steel strands with the aid of the wavelet transform", *Smart Mater. Struct.*, **14**, 685-695.
- Rizzo, P. and Lanza di Scalea, F., (2005b), "Discrete wavelet transform for enhancing defect detection in strands by guided ultrasonic waves", *Int. J. Struct. Health Monitoring* in press.
- Sohn, H., Farrar, C.R., Hunter, N.F. and Worden, K. (2001), "Structural health monitoring using statistical pattern recognition techniques", *J. Dynamic Systems, Measurement, and Control*, ASME, **123**, 706-711.
- Staszewski, W., Pierce, G., Worden, K., Philp, W., Tomlinson, G. and Culshaw, B. (1997), "Wavelet signal processing for enhanced Lamb-wave defect detection in composite plates using optical fiber detection", *Optical Eng.*, **36**(7), 1877-1888.
- Staszewski, W. (1998), "Wavelet based compression and feature selection for vibration analysis", *J. Sound Vib.*, **211**, 735-760.
- Staszewski, W., (2002), "Intelligent signal processing for damage detection in composite materials", *Composites Science and Technology*, **62**, 941-950.
- Staszewski, W., Boller, C. and Tomlinson, G. (2004), *Health Monitoring of Aerospace Structures*, John Wiley & Sons, Munich, Germany.
- Washer, G. A., Green, R. E. Jr. and Pond, R. B. Jr. (2002), "Velocity constants for ultrasonic stress measurement

- in prestressing tendons”, *Research in Nondestructive Evaluation*, **14**, 81-94.
- Watson, S. C. and Stafford, D. (1988), “Cables in trouble”, *Civil Engineering*, **58**(4), 38-41.
- Woodward, R.J. (1988), “Collapse of Ynys-y-Gwas bridge, West Glamorgan”, *Proceedings - Institution of Civil Engineers*, **84** (Part 1), 635-669.

FC